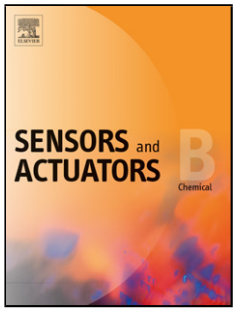
Accepted Manuscript



Title: On-Chip Microelectrode Array and In-Situ Transient Calibration for Measurement of Transient Concentration Gradients Near Surfaces of 2D Cell Cultures

Author: Siddarth V. Sridharan Jose F. Rivera James K. Nolan Muhammad A. Alam Jenna L. Rickus David B. Janes

PII: S0925-4005(17)32530-3
DOI: https://doi.org/doi:10.1016/j.snb.2017.12.194
Reference: SNB 23882

To appear in: *Sensors and Actuators B*

Received date: 8-11-2017
Revised date: 29-12-2017
Accepted date: 30-12-2017

Please cite this article as: Siddarth V. Sridharan, Jose F. Rivera, James K. Nolan, Muhammad A. Alam, Jenna L. Rickus, David B. Janes, On-Chip Microelectrode Array and In-Situ Transient Calibration for Measurement of Transient Concentration Gradients Near Surfaces of 2D Cell Cultures, *<![CDATA[Sensors & Actuators: B. Chemical]]>* (2018), https://doi.org/10.1016/j.snb.2017.12.194

This is a PDF file of an unedited manuscript that has been accepted for publication. As a service to our customers we are providing this early version of the manuscript. The manuscript will undergo copyediting, typesetting, and review of the resulting proof before it is published in its final form. Please note that during the production process errors may be discovered which could affect the content, and all legal disclaimers that apply to the journal pertain.

ACCEPTED MANUSCRIPT

On-Chip Microelectrode Array and In-Situ Transient Calibration for Measurement of Transient Concentration Gradients Near Surfaces of 2D Cell Cultures

Siddarth V. Sridharan[a,b,1], Jose F. Rivera[a,b,1], James K. Nolan[c,b], Muhammad A. Alam[a,b], Jenna L. Rickus[c], David B. Janes[a,b,*]

[a] *Electrical and Computer Engineering, Purdue University, West Lafayette, IN 47907, USA.*
[b] *Birck Nanotechnology Center, Purdue University, West Lafayette, IN 47907, USA.*
[c] *Agricultural and Biological Engineering, Purdue University, West Lafayette, IN 47907, USA*

Abstract

Amperometric microelectrode arrays (MEAs) interrogate the concentration at multiple positions simultaneously and with sufficient sampling rates, thus being able to capture fast transient gradients. However, sensitivity variability issues in amperometric MEAs degrade the reliability of the measurements, particularly at the small concentration scales found in physiological studies. This paper describes the development of on-chip platinum amperometric MEAs and in-situ transient calibration for reliable measurement of physiological transient concentration gradients. The designed MEA geometry facilitates positioning near a 2D cell culture setup, and the proposed in-situ transient calibration minimizes the effects of sensitivity variability, thus allowing for calculation of gradients based on concentration differences between closely spaced electrodes. The effectiveness of the MEA and the in-situ transient calibration was evaluated by measuring controllably-generated gradients, and then calculating the difference between experimental and simulated data using normalized time analysis. Gradients generated by periodic uptake intervals as fast as 150 ms followed by recovery intervals of 60 s were measured over a spatial range of 70 μm, with spatial resolution of 35 μm, and

*Corresponding author
Email address: janes@purdue.edu (David B. Janes)
[1] These authors contributed equally to this work.

ACCEPTED MANUSCRIPT

sampling time and measurement time of 10 ms. Transient gradients of hydrogen peroxide were also measured above the surface of a 2D cell culture of human astrocytes, thus demonstrating the approach in actual physiological measurements.

Keywords: Microelectrode Array, Amperometric Sensing, Hydrogen Peroxide, Concentration Gradient, Concentration Transients, 2D Cell Culture, Human Astrocytes, Cellular Gradients, Biosensors, Platinum Electrodes.

1. Introduction

Concentration gradients are crucial in many biological processes [1, 2, 3, 4, 5, 6, 7, 8, 9, 10] at the single-cell, tissue, and organ levels. Cells act as sources and sinks of molecules via release and uptake processes, respectively, resulting in concentration gradients in the extracellular space. In adherent 2D cell cultures, these uptake/release processes generate concentration gradients exhibiting spatial scales of hundreds to thousands of microns with time scales ranging from steady-state to millisecond regimes, and local concentration changes going up to a few hundreds of μM [11, 12, 13, 14, 15]. The magnitude, direction, and time scales of the gradients from the cell surface carry information that is communicated both internally to the cell and externally to neighboring cells.

Gradient measurements require accurate absolute concentration values at various spatial positions to allow for quantitative determination of critical physiological information such as diffusive fluxes [16, 3, 2, 17], uptake/release kinetics [18, 19, 20], influence radii [21, 6] and local concentration dependencies [16, 12]. Obtaining information about the sink/source dictates that the sensing positions must be within the transient spatial scale (also known as depletion/accumulation width) of the dynamic gradient. In the context of gradient measurements, the relevant spatial and temporal quantities are the spatial range, defined as the distance between the nearest and farthest measurement positions with respect to the source/sink; the spatial resolution, defined as the distance between each measurement position; the sampling time, defined as the time interval between data points; and the measurement time, defined as the time it takes to obtain quantitative concentration information over the entire spatial range. In general, the shortest transient gradient that can be measured is limited by the measurement time.

ACCEPTED MANUSCRIPT

Techniques such as the vibrating probe self-referencing technique (SRT) [1, 22, 23, 17, 24, 25, 2] have been employed to measure biomolecule gradient/flux from cell surfaces using a single biosensor oscillating between two sensing positions separated by a fixed distance (Fig. 1). While SRT techniques can obtain data over reasonably large spatial ranges, the measurement time is much longer than the sampling time due to the restrictions on tip velocity to avoid stirring and the required number of oscillations for lock-in detection [23, 17, 24, 25, 2]. Acquisition of gradient information at multiple spatial locations requires multiple measurements, typically over tens of seconds, even with rapid sampling times (μs or ms scale) and high spatial resolution (nm scale). Techniques such as scanning electrochemical microscopy (SECM) also have high spatial resolution (nm scale) and short sampling times (μs or ms scale) [26, 27, 28, 29, 30]; however, in the context of gradient measurements, the multi-point measurements also result in relatively large measurement times due to the restrictions on scan rate (typically 8-25 μm s^{-1}) [26, 12] in order to avoid disruption of the gradient via induced convection [26, 31]. Moreover, optical techniques involving a fluorescent dye that binds to the analyte of interest have been employed to make concentration sampling over the entire reaction volume. While optical techniques have been used to image a concentration gradient of an electroactive fluorescent molecule near a 2D sink electrode [32], such techniques have not been extended to analytes of biological interest. The lack of reversible optical probes for analytes of biological significance like hydrogen peroxide has been identified as a limiting factor in extracellular measurements [33].

Individually addressed microelectrode arrays (MEAs) provide customizable spatial range and short measurement times by simultaneously measuring at multiple sensor electrodes. Amperometric MEAs have been used to demonstrate real time imaging of various non-physiological transient gradients that were set up by injecting or flowing highly-concentrated solutions (10-1000 mM) within or near a 2D MEA [34, 35, 36, 37, 38]. Amperometric MEAs have also been used for purposes other than gradient measurements, e.g., detection of exocytotic release from both single cells [39, 40] and clusters of cells scattered on the MEA surface [41, 42, 43, 44, 45, 46]. To date, MEAs have not been widely used to study concentration profiles/gradients in the vicinity of 2D cell cultures or other common culture geometries. Even in measurements involving artificial (non-physiological) gradients, many reports present raw current data or rise times rather than absolute concentration values, thereby preventing the quantification of gradients. Several factors are

ACCEPTED MANUSCRIPT

believed to limit the ability to quantify gradient information. First, the MEA substrate geometry and packaging typically are not optimized for positioning the electrodes along a gradient field in proximity to a 2D cell culture or artificial analog thereof. Second, sensitivity variability hinders the determination of absolute concentrations at multiple electrodes with sufficient accuracy. Sensitivity variability in the forms of "response variability" (when sensitivity changes from experiment to experiment) and "sensitivity drift" (when sensitivity changes during the time course of an experiment) are inherent to amperometric sensing [47, 48, 49, 50, 42, 44]. Additionally, MEAs exhibit "electrode variability", i.e., sensitivity changes among electrodes in the array. Evidence from the literature indicates that typical values of "electrode variability" [41, 35, 43, 36, 42, 37, 38] and "response variability" [51, 36, 52] are between 10-20%. Although "sensitivity drift" is common in the literature of single electrodes [47, 48, 49], data in previous MEA reports show clear evidence of sensitivity drift [41, 42, 44]. As the background concentrations become smaller (e.g., < 1 mM), the three categories of sensitivity variability make it difficult to determine concentrations at multiple electrodes with sufficient accuracy to calculate gradients based on concentration differences (ΔC) between pairs of adjacent electrodes.

This study showcases the quantitative measurement of transient gradients using amperometric 1D MEAs and in-situ transient calibration. The MEAs were designed in a geometry suitable for measurements of gradients in conventional 2D cell culture setups. The proposed in-situ transient calibration minimizes the aforementioned effects of sensitivity variability via the in-situ acquisition of sensitivity factors for each electrode in the array just prior to capturing the transient of interest. This approach to measuring gradients could be considered a hybrid between SRT and traditional 2D MEAs, allowing acquisition of quantitative gradient information at multiple locations with measurement times significantly faster than typical SRT approaches (Fig. 1). A planar large sink electrode (LSE) is used to controllably induce dynamic gradients of hydrogen peroxide (H_2O_2) by consuming H_2O_2 upon excitation (Fig. 2). This LSE geometry mimics a 2D cell assembly, e.g., a monolayer of astrocytes [11, 13], endothelial cells [14] or bacteria [12], consuming H_2O_2 from the surroundings. Transients/gradients generated by the LSE were characterized experimentally, and the reliability of the measurements was assessed by comparing experimental and numerical data via normalized time analysis. In contrast to previous MEA reports, the current study focuses on gradients that are characterized by smaller background con-

ACCEPTED MANUSCRIPT

centration scales (20 μM to 1 mM), short to long transients (150 ms-1000 s), and most importantly, small local concentration differences (ΔC down to sub-μM scale). Finally, the application of the approach to a physiological system is demonstrated by measuring H_2O_2 concentration transients near a 2D cell culture of human astrocytes and determining the associated gradients.

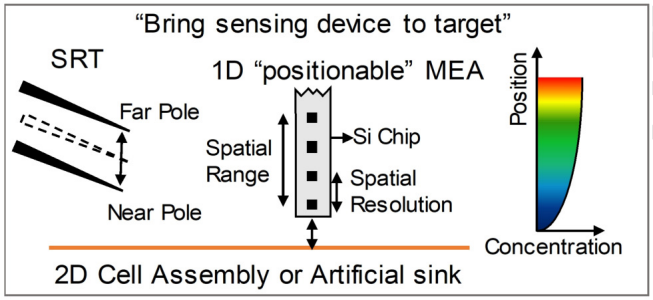


Figure 1: **Analyte sink induces a concentration profile (rainbow colored) where concentration increases with position with respect to the sink. A positionable MEA (1D in this work) interrogates simultaneously all the electrodes within a desired spatial range every 10 ms, thus yielding a measurement time suitable for quantifying gradients induced by sub-second events in a "single-shot" measurement.** Vibrating probe techniques like SRT (left) acquire gradient information at a single spatial location by oscillating the probe tip between near and far poles. Even at a single spatial location, measurement times are typically much greater than sampling time due to restricted oscillation frequency (typically less than 1 Hz), required to keep the tip velocity below the level that disrupts the gradient of interest, and due to the need for measurements over multiple oscillation periods. The use of an MEA with appropriate electrode size and spatial range, along with in-situ calibration approach, allows measurements of concentration transients at various electrode locations, and determination of local gradients/fluxes near artificial or physiological (e.g. common 2D cell/tissue culture geometries) planar sinks of analytes.

2. Materials and methods

2.1. Reagents

Hydrogen peroxide 30% (w/w) was purchased from Alfa Aesar (Ward Hill, MA) and phosphate buffer saline (PBS) pH 7.4 was purchased from Sigma-Aldrich (St. Louis, MO). All H_2O_2 solutions were prepared with 0.01 M PBS in ultrapure water. Human cerebral cortex astrocytes, astrocyte medium, cell freezing medium and 10 mg/ml poly-L-lysine were purchased

ACCEPTED MANUSCRIPT

from ScienCell Research Laboratories (Carlsbad, CA). Astrocyte medium contained 500 ml of basal medium, 10 ml of fetal bovine serum (FBS, Cat. No. 0010), 5 ml of astrocyte growth supplement (AGS, Cat. No. 1852) and 5 ml of penicillin/streptomycin solution (P/S, Cat. No. 0503). Glucose solution (50 ml of 200 g/L) and 4-well chambered cover glass systems with 1.0 borosilicate glass were purchased from Thermo Fisher Scientific (Waltham, MA).

2.2. MEA design and fabrication

For the non-physiological measurements, the MEA consists of a 1D array of three electrodes (5 μm $\times$ 5 μm) with inter-electrode separation of 35 μm center-to-center (or 30 μm edge-to-edge). Electrodes are located very close (30 μm) to the bottom edge of the silicon die, and designated E1, E2 and E3, where E1 is the electrode closest to the edge. Fig. S-1 in Supplementary Material shows the details of the MEA design and fabrication process. For the physiological measurements, the MEA consists of a 1D array of five electrodes (10 μm $\times$ 10 μm) with inter-electrode separation of 140 μm center-to-center, which allows for measurements over a larger spatial range of the concentration profile ($\sim$600 μm).

2.3. Apparatus

Multiple potentiostats (Reference 600, Gamry Instruments Inc., Warminster, PA) were employed to individually bias the electrodes in the array and the LSE; the latter consisted of a platinum disk electrode (1.6 mm diameter). Platinum wire and disk (0.5 mm and 1.6 mm diameter, respectively) were used as counter electrodes; the wire was shared among the sensing electrodes in the array, while the disk was the auxiliary for the LSE. Two Ag/AgCl (sat'd 3M NaCl) reference electrodes were used; the sensing electrodes in the array shared a single reference electrode. Both the counter electrodes, LSE and reference electrodes were purchased from BASI Inc. (West Lafayette, IN). For the measurements with cultured human astrocytes, only the sensing electrodes in the MEA were used. Unless stated otherwise, all potentials are referred to the Ag/AgCl (sat'd 3M NaCl) reference electrode, and all experiments were performed at room temperature.

2.4. MEA characterization

Cyclic voltammetry of 0.5 mM H_2O_2 in 0.01 M phosphate buffered saline was used to characterize the oxidation peak of H_2O_2 at Pt surface, which was

ACCEPTED MANUSCRIPT

found to be 0.5 V. For initial characterization, the amperometric response of the electrodes to concentrations ranging from 0 to 1.2 mM H_2O_2 were recorded by immersing the MEA chip in various unstirred H_2O_2 solutions (6 mL) followed by biasing the electrodes at 0.5 V. The obtained data were used to evaluate linearity, transient sensitivities, and electrode-to-electrode variabilities. For all concentration transient/gradient measurements, the electrodes were calibrated via in situ transient calibration procedure, as described in Section 2.6.

2.5. Geometry for transient and gradient measurements with LSE

The silicon chip with the MEA was manually brought into proximity to the LSE surface (Fig. 2) such that the three sensor electrodes were aligned perpendicular to the surface of the LSE and centered within the area of the LSE. Using optical microscopy, the distances z_i between the LSE surface and the center of each electrode E_i (i = 1, 2, 3) were found to be $z_1 \approx 165$ μm, $z_2 \approx 200$ μm and $z_3 \approx 235$ μm (Fig. 2). Once the chip was placed in position, all the experiments were run in sequence without movement of the chip with respect to the LSE. A Petri dish containing 6 mL 0.01M phosphate buffer saline with uniform concentration of 1 mM H_2O_2 was used throughout the measurements.

2.6. In situ transient calibration and measurement of transient concentrations and their gradients

With the MEA chip positioned as described in Section 2.5, the three MEA electrodes were biased at 0.5 V starting from t = 0 s and throughout the course of an experiment. Every electrode i in the array provides a current $I_i(t)$ due to the time-dependent local concentration at the position z_i perpendicular to the LSE surface. No bias was applied to the LSE during the first 300 s, such that the amperometric data corresponded to the electrode responses to the uniform concentration of 1 mM H_2O_2. Taken together, the known H_2O_2 concentration (C_0 = 1 mM) and the electrode currents at t = 300 s (called I_{300}) were subsequently used to convert $I_i(t)$ from each electrode into a spatially-resolved concentration vs. time, namely $C_i = C(z_i, t) = (C_0/I_{300})_i \times I_i(t)$, where $(C_0/I_{300})_i$ is the sensitivity factor for electrode i. This procedure is denoted in situ transient calibration. The settling time of 300 seconds was chosen to reduce the sensitivity drift to a level (1.7% min^{-1}) that allows measurement of transient response over several minutes,

ACCEPTED MANUSCRIPT

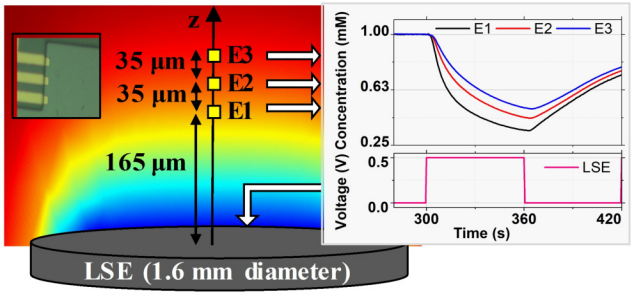


Figure 2: **Schematic of experimental setup, not drawn to scale. Large sink electrode (LSE) controllably generates a concentration field (indicated by color scale) with associated gradients as a function of time and position, and in response to a potential of 0.5 V applied between 300-360 s (see inset). This diffusion-reaction system emulates a 2D assembly of cells consuming analyte from the surroundings, and constitutes the benchmark to evaluate the performance of the microelectrode array (MEA) as a reliable tool for measurement of physiological gradients.** Platinum microelectrodes E1, E2 and E3 (5 μm $\times$ 5 μm each) in the MEA are one-dimensionally arranged with inter-electrode separation of 35 μm (center-to-center). MEA packaging allowed positioning of E1 at 165 μm from the LSE. These microelectrodes record changes in local concentration at positions 165, 200, and 235 μm with respect to the LSE via amperometric signals, which are later converted into concentration data. The spatial dependence of the concentration field dictates that concentration increases with distance from LSE. Left inset shows photograph of the three microelectrodes in the MEA. Right inset shows concentration transients obtained simultaneously from the three microelectrodes in response to a potential of 0.5 V applied to the LSE between 300-360 s followed by a recovery interval from 360-420 s. The concentration was uniform and constant at 1 mM before 300 s. The spatial dependence of the concentration field dictates that concentration increases with distance from LSE, as indicated by the order E1 $<$ E2 $<$ E3 in the concentration amplitudes. This systematic behavior indicates that each microelectrode records the concentration transient locally.

ACCEPTED MANUSCRIPT

as determined by a separate experiment involving monitoring of the electrode sensitivities over approximately 2000 seconds.

Immediately after, starting at t = 300 s, time-dependent gradients were generated electrochemically by applying a sequence of four potential pulses to the LSE, consisting of voltages of 0.5 V during the interval t_{uptake} and open circuit potential during the interval $t_{recovery}$; hence, the pulse period was $t_{pulse} = t_{uptake} + t_{recovery}$. The interval t_{uptake} was set at 0.15, 1, 10 or 60 s for a given experiment, and the time $t_{recovery}$ was kept constant at 60 s for all the experiments. The local time-dependent gradient was calculated as $G_{i+1,i} = (C_{i+1} - C_i)/\Delta z$, where Δz is the distance between z_i and z_{i+1} in the direction perpendicular to the LSE surface. The $G_{i+1,i}$ is associated with the position at half the distance between z_i and z_{i+1}. From this result, the diffusive flux $J_{i+1,i}$ is calculated by invoking Fick's second law as $J_{i+1,i} = -D\ G_{i+1,i}$, assuming that the H_2O_2 diffusion coefficient D is 1.71×10^{-5} $cm^2\ s^{-1}$ [53]. This methodology is a logical extension of the self-referencing technique (SRT), which has shown that the numerical value of $G_{i+1,i}$ is a good approximation to the actual local gradient as long as Δz is small enough to ensure the linearity of the gradient between z_i and z_{i+1} [1, 17]. Typically, gradient measurements using SRT have been performed with $\Delta z \sim 30\ \mu m$ [23, 17, 24, 25, 2].

2.7. Numerical model

Numerical solution of a diffusion-reaction model was performed using Comsol Multiphysics to resolve the spatio-temporal changes in the concentration profile as a function of the potential pulses applied to the LSE. Due to the cylindrical symmetry of the problem, the geometry of the Petri dish corresponds to the volume enclosed by r = 20 mm and $0 \leq z \leq 10$ mm, and the geometry of the circular LSE corresponds to the surface enclosed by r = 0.8 mm at z = 0. Therefore, a two-dimensional solution of the diffusion equation in cylindrical coordinates with surface reactions occurring at both the LSE and the sensing electrodes was sufficient to resolve the physics of the problem. The diffusion coefficient of H_2O_2, 1.71×10^{-5} $cm^2\ s^{-1}$, was obtained from the literature [53], and the heterogeneous reaction rate constant (k_F) of the LSE was adjusted to fit the experimental data.

2.8. Cell culture

Human cerebral cortex astrocytes were obtained from Sciencell (Carlsbad, CA) cryopreserved at passage one. Astrocytes were expanded and maintained

ACCEPTED MANUSCRIPT

per the company's protocol. For each experiment, passage three astrocytes (5.0×10^4 cells cm^{-2}) were seeded onto poly-L-lysine-coated chambered cover glass system wells and incubated for two days in a humidified atmosphere containing 5% CO_2 at 37°C. Medium was replaced with fresh astrocyte medium one day after seeding. Cells were used for gradient measurements after two days of incubation. Prior to the gradient measurements, the cultures were washed twice with PBS (pH 7.4), and then 0.3 mL of 5.5 mM glucose in PBS was added to culture well.

2.9. Geometry and timeline for transient and gradient measurements with cultured human astrocytes

For the physiological experiments, a MEA with different dimensions (10 μm × 10 μm electrodes with a 140 μm pitch) was used to enable measurements over the temporal and spatial ranges of interest for H_2O_2 consumption by the cells. In addition, an alternative approach for establishing the starting time for H_2O_2 consumption and performing in-situ transient calibration was developed, as follows. The MEA was initially positioned over the cell culture, such that the bottom of the chip was 5 mm from the cell surface. Initially, the cell culture contained 0.3 mL of 5.5 mM glucose in PBS. At t = 0 s, 1.2 mL of solution containing 25 μM H_2O_2 and 5.5 mM glucose in PBS was added to obtain 1.5 mL of solution with final concentrations of 20 μM H_2O_2 and 5.5 mM glucose in PBS. At t = 30 s, the five electrodes in the MEA were simultaneously biased at 0.5 V; this bias was maintained throughout the course of the experiment. The amperometric response was allowed to settle for 300 s; then the current at each electrode at t = 330 s was used to determine the in-situ sensitivity factor for that electrode. Based on modeling of the diffusion profile using the inferred consumption rate of peroxide (and confirmed by the experimental results), the diffusion profile has not yet reached the position of the MEA electrodes at t = 330 s, so the concentration at the location of the MEA is the background concentration of 20 μM. Just after the measurement at t = 330 s, the MEA was moved using a XYZ micro-positioner to a position such that the distances z_i between the cell culture surface and the center of each electrode E_i (i = 1, 2, 3, 4, 5) were $z_1 \approx 60$ μm, $z_2 \approx 200$ μm, $z_3 \approx 340$ μm, $z_4 \approx 480$ μm and $z_5 \approx 620$ μm. The transient measurements started immediately thereafter, and the current at each electrode was converted into a concentration using the corresponding in-situ sensitivity factor. Concentration measurements at all five electrodes were obtained in a single measurement run, and gradients were

ACCEPTED MANUSCRIPT

calculated at each time point from the corresponding concentration values, without smoothing or multi-point averaging.

3. Results and Discussion

3.1. MEA device characterization

Amperograms of ultramicroelectrodes typically exhibit an initial transient response (settling time) before achieving steady state, and conventional calibration methods use the values of steady state current to extract sensitivities. In our experiments, the amperograms of the electrodes biased at 0.5 V were monitored for 2000 s without observing steady state currents (Fig. S-2 in Supplementary Material). This effect, interpreted as a drift in sensitivity and observed in other MEA [42, 44] and single-electrode [47, 48, 49] studies, precluded the extraction of conventional steady state sensitivities. Alternatively, sensitivity was obtained by plotting the current measured at t = 300 s (called I_{300}) vs. the concentration present in the solution (0, 0.2, 0.4, 0.8 and 1.2 mM H_2O_2), for each electrode in the array (Fig. S-3 in Supplementary Material). This time point (t = 300 s) was chosen to provide a good trade-off between settling time and average rate of sensitivity drift, which was found to be 1.7% min^{-1} (see discussion of Fig. S-2 in Supplementary Material). The data of I_{300} vs. concentration (shown in Fig. S-3 in Supplementary Material) were used to assess linearity and to determine sensitivity (called S_{300} as it is associated to I_{300}) and limit of detection for each electrode. Linear fitting provided S_{300} values of 2.07 ± 0.11, 1.44 ± 0.05 and 1.47 ± 0.06 nA mM^{-1} (mean ± standard error, n = 3) for E1, E2 and E3, respectively, and the corresponding R-square values were always above 0.99, indicating that the three electrodes in the array are linear over the range of interest (0-1.2 mM). The average sensitivity ± standard deviation was 1.65 ± 0.36 nA mM^{-1}, yielding electrode variability of 21.8%, whereas the response variability from triplicate experiments was found to be 2.5%. In order to avoid the need for selectivity, the experiments were performed with media containing only H_2O_2 and buffered inert electrolyte (phosphate buffer saline), as has been common in prior reports [54, 55, 16, 56, 57, 13, 15, 58]. However, our approach can be applied to the sensing of other analytes and can incorporate typical approaches for achieving selectivity through enzymatic and nanostructured functionalizations [59, 60, 50, 61, 25, 17, 23, 24, 2, 62].

ACCEPTED MANUSCRIPT

3.2. In situ transient calibration

Characterization of the MEA indicates that the electrode variability (21.8%) and the response variability (2.5%) are large enough to prevent accurate determination of dynamic gradients based on concentrations quantified by the traditional MEA calibration (see Supplementary Material for a description of the traditional MEA calibration). Therefore, in situ transient calibrations were performed, as described in Section 2.6, to obtain calibration factors immediately prior to applying a potential pulse waveform or prior to approaching the chip to the cell surface. The in situ transient calibration minimizes both response variability and sensitivity drift by obtaining a calibration factor for every experiment "in situ" just prior to the generation of the gradient of interest, and minimizes electrode variability by performing an individual calibration of each electrode in the MEA. This approach could be viewed as a multi-electrode version of in situ calibration approaches previously used to interpret single electrode experiments [26, 16]. Like the conventional single point calibration, the in situ transient calibration relies on response linearity and negligible offset, as established by the data of I_{300} vs. concentration, and works well for concentration transients that change more rapidly than the sensitivity drift rate (see discussion of Fig. S-2 in Supplementary Material).

3.3. Spatio-temporal resolution of transient concentrations using the MEA

Fig. 2 shows the schematic diagram of a diffusion-reaction system constituted by an LSE surrounded by H_2O_2 solution. This system was used to controllably generate transient gradients by applying potential pulse waveforms to the LSE, and the generated gradients were measured by the MEA. A potential pulse waveform comprises four pulses, and each pulse consists of an interval (t_{uptake}) with potential at 0.5 V followed by an interval ($t_{recovery}$) at open circuit potential. During the interval t_{uptake}, the LSE electro-oxidizes (i.e., consumes) H_2O_2 causing a depletion in concentration. During the interval $t_{recovery}$, the depleted solution adjacent to the LSE recovers progressively toward the initial concentration due to diffusion from the bulk solution. Fig. 2 (right inset) shows the processes of depletion and recovery of the concentration near the LSE in response to a single pulse applied to the LSE. In this case, the background concentration is 1 mM, the pulse starts at t = 300 s and has t_{uptake} and $t_{recovery}$ equal to 60 s, and the concentrations at the positions of the electrodes display transient behaviors consistent with depletion and recovery. Similar results for a single pulse having t_{uptake} = 1 s and $t_{recovery}$ = 60 s in 20 μM background concentration are shown in Fig. S-4 in

ACCEPTED MANUSCRIPT

Supplementary Material. Note that other reports on gradient measurements using amperometric MEAs have worked with concentrations in the range of 10-1000 mM [34, 35, 36, 37, 38] whereas the expected physiological concentrations of H_2O_2 are below 1 mM [63]. Since sensitivity variability is more detrimental at small concentrations, the above results indicate that MEA and in situ transient calibration, altogether, are effective at physiological concentrations.

Fig. 3A and 3C show the transient concentrations for potential pulse waves with t_{uptake} of 0.15 and 60 s. Corresponding results for pulse waves with t_{uptake} of 1 and 10 s are shown in Fig S-5 in Supplementary Material. In these four cases, $t_{recovery}$ is 60 s and the positions of the sensors with respect to the LSE are 165, 200, and 235 μm, as illustrated in Fig. 2. The systematic change in signal waveforms at various electrodes, and the order in the signal amplitudes (E1 < E2 < E3), indicate that each sensor captures the concentration dynamics locally, with spatial resolution given by the inter-electrode separation (35 μm).

Experimental curves in Fig. 3A and 3C agree well with the simulated curves shown in Fig. 3B and 3D, respectively. These results indicate that the intrinsic response time of each individual electrode is fast enough to resolve the transient concentrations arising from uptake events as short as 0.15 s. This ability to measure gradients caused by rapid (e.g., sub-second) uptake events in stagnant solution is a major advantage of MEAs over scanning probe techniques. The good agreement between experimental and numerical results also indicates that accurate quantification of concentration is possible via the in situ transient calibration, wherein the currents corresponding to a known background concentration (in this case, 1 mM) are measured for each electrode just prior to the onset of the uptake event. In contrast, the concentrations quantified via the traditional MEA calibration do not agree with the numerical predictions neither qualitatively nor quantitatively, as shown in Fig. S-6 (B and E) in Supplementary Material.

Altogether, the above results differ from other amperometric MEA reports in various aspects. First, all the measured transients are due to diffusion, as the solution is stagnant, whereas in other reports the transients are due to flow or injection of analyte [34, 35, 36, 37]. Second, all the measurements are performed in the direction perpendicular to the active surface. This geometry is consistent with the direction of mass transport in 2D adherent cell cultures [2]. Third, the signals are quantified in absolute concentration scale. Absolute concentration values allow for quantitative determination of critical

ACCEPTED MANUSCRIPT

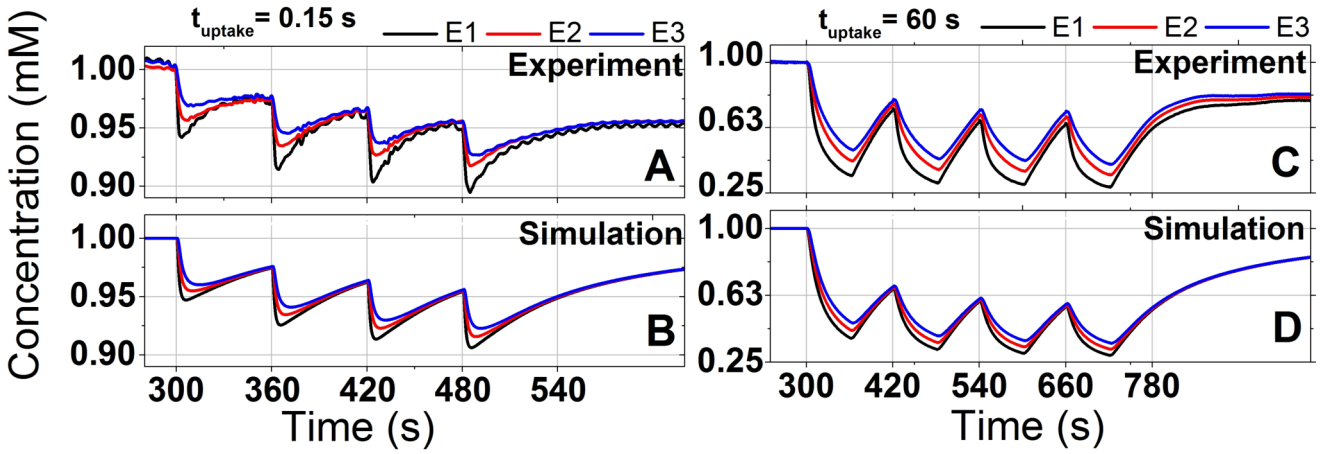


Figure 3: **Simultaneous concentration measurements were obtained at multiple electrodes, thus capturing transients induced by the LSE in response to uptake intervals as short as 0.15 s (left). Experimental curves (A, C) agree well with corresponding numerical simulation results (B, D) over most of the temporal scale of the experiments.** The plotted curves indicate concentrations measured at electrodes E1 (165 μm), E2 (200 μm) and E3 (235 μm) in response to potential pulse waves applied to the LSE, starting at t = 300 s. Each wave comprises four pulses, and each pulse has duration $t_{pulse} = t_{uptake} + t_{recovery}$, with $t_{recovery} = 60$ s for all the pulse waves. (A, B) $t_{uptake} = 0.15$ s, (C, D) $t_{uptake} = 60$ s. The concentration was uniform and constant at 1 mM before 300 s.

physiological information such as diffusive fluxes [16, 3, 2, 17], uptake/release kinetics [18, 19, 20], influence radii [21, 6] and local concentration dependencies [16, 12]. Fourth, the experiments addressed measurements of uptake intervals as short as 150 ms, thus paving the way toward the study of rapid transient gradients in, for instance, in vitro cell networks [2, 64].

3.4. Dynamic gradients and fluxes of hydrogen peroxide

Transient gradients were obtained by calculating the difference in the measured transient concentrations between pairs of adjacent electrodes, as described in Section 2.6. Fig. 4 shows the transient gradients for potential pulse waves with t_{uptake} of 0.15 and 60 s. Corresponding results for pulse waves with t_{uptake} of 1 and 10 s are shown in Fig. S-7 in Supplementary Material. The peak of the gradient inferred from the concentration difference between E1 and E2 is larger than that inferred from E2 and E3, as expected from the relative positions with respect to the LSE. The gradients

ACCEPTED MANUSCRIPT

are presented here in units of μM μm^{-1}, which are particularly useful for intuitive understanding of physiological scenarios; other relevant units such as mol cm^{-4} can be obtained using appropriate conversion factors. Using diffusion coefficients from the literature, the calculated gradients can be converted to diffusive fluxes, with peak amplitudes in the range of 34-625 pmol cm^{-2} s^{-1}. Fluxes exhibiting peak amplitudes in the range of 2-5 pmol cm^{-2} s^{-1} were also measured for background concentration of 20 μM (Fig. S-4 in Supplementary Material). These experimental results are in the same order of magnitude as reported physiological measurements. For instance, data from literature allows to calculate an average H_2O_2 influx of 29 pmol cm^{-2} s^{-1} for a monolayer of human breast cancer cells (MDA-MB-231, 2.1×10^5 cells distributed on a circular surface of 6.35 mm diameter) [13], and other report quoted H_2O_2 influx of 10 pmol cm^{-2} s^{-1} for bacteria biofilm.[12] These gradient measurements illustrate the potential of the MEA as an analytical tool for physiological studies.

3.5. Numerical Simulation

Calculation of transient gradients requires reliable measurements of transient concentrations. The reliability of the measurements was assessed via predictions based on the well-known diffusion-reaction model [65, 49, 66, 67, 68, 69], which allows for computation of the local concentration profile as well as the corresponding transient concentrations at the positions of the sensor electrodes. The diffusion-reaction model sets the reaction flux occurring at the active surface (in this case, the LSE surface) to be proportional to the local concentration, with proportionality constant k_F (also known as heterogeneous reaction rate constant). As previously shown in Fig. 3, the simulated curves (panels B and D) agree qualitatively and quantitatively with the corresponding experimental curves (panels A and C) when k_F is set at 10^{-2} cm s^{-1}, thus indicating that explicit information about the active surface can be obtained by fitting the simulation to the experimental data. This strategy to obtain information about the active surface has been discussed theoretically [3].

The overall behavior within a pulse wave can be understood by considering Fig. 5, which presents simulated concentration profiles for t_{uptake} of 60 and 0.15 s. Each curve corresponds to a specific time point within the pulse waveform, as indicated by symbols in the corresponding insets, and the shaded bands represent the distance range (150-250 μm) wherein the electrodes were located during the experiments. When the LSE is biased at 0.5 V

ACCEPTED MANUSCRIPT

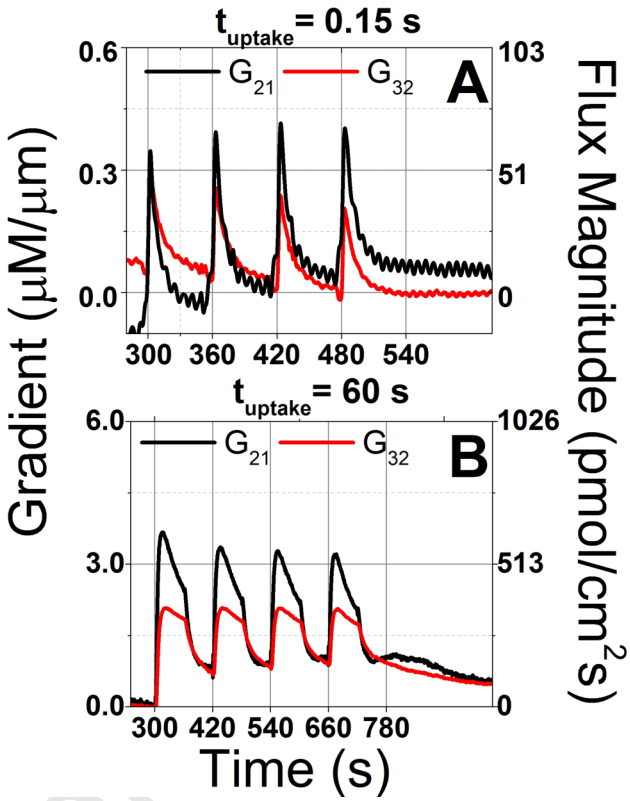


Figure 4: **Reliable concentration data from multiple electrodes allow for determination of transient gradients based on the concentration differences between pairs of adjacent electrodes. In situ transient calibration provides the required reliability by reducing the effects of sensitivity variability.** The plotted curves indicate the gradients obtained from computation of the concentration difference between E1−E2 (G_{21}), and E2−E3 (G_{32}) in response to potential pulse waves applied to the LSE. (A) t_{uptake} = 0.15 s, (B) t_{uptake} = 60 s. For all pulse waves, $t_{recovery}$ = 60 s. Corresponding diffusive flux magnitudes can be read from the right scale axis. Peak diffusive flux magnitudes are in the range of 34-625 pmol cm^{-2} s^{-1}. These experimental results are in the same order of magnitude as reported physiological measurements.

ACCEPTED MANUSCRIPT

(uptake intervals), the electro-oxidation of H_2O_2 takes place at the LSE surface with a high rate constant k_F, so the concentration near the LSE becomes depleted. When the LSE is left at open circuit potential (recovery intervals), negligible electro-oxidation reaction occurs at the LSE surface, and the concentration near the LSE recovers progressively toward initial concentration due to diffusion from the bulk solution. The profile recovery is only partial for all the recovery intervals, i.e., the concentration profile never recovers the initial functional form (indicated by curves in black-filled symbols). Consequently, deeper diffusion profiles are induced pulse after pulse. This behavior indicates that, for the diffusion-reaction system studied here, each potential pulse within the studied pulse waves yields a unique concentration profile. Accordingly, the concentrations at the positions of the electrodes (i.e., within the shaded bands in Fig. 5) exhibit a decreasing trend from one pulse to another. This trend is captured quantitatively by the MEA, as shown in Section 3.3. To better assist the comprehension of spatiotemporal propagation of uptake events occurring at the LSE surface, simulated 3D plots of concentration as a function of time and distance from the LSE, and in response to single pulses with t_{uptake} of 60 and 0.15 s, are shown in Figure S-8 in Supplementary Material.

3.6. Diffusional Distortion and Normalized Time Analysis of Spatial and Temporal Response

Although consumption of H_2O_2 at the LSE starts immediately after the voltage pulse is applied, the corresponding depletion of analyte at the location of the MEA electrodes does not happen instantaneously. Therefore, extracting information about the events occurring at the active surface requires an approach to account for the delay time t_0 caused by diffusion between the LSE surface and the electrode locations. This phenomenon, known as diffusional distortion [70], is used here to interpret the time-dependent measurements obtained at known distances from the LSE. Note that the delay time t_0 is a position-dependent quantity and is an inherent characteristic of diffusion-reaction systems. It should not be mistaken for the response time of the electrodes in the MEA.

The analytical expression for the measured transient concentrations has the general functional form $C/C_0 = f(t_{uptake}, t_{recovery}, D, z, t)$, where C_0 is the initial background concentration, D is the diffusion coefficient, z is the position with respect to the active surface, t is the time, and t_{uptake} and $t_{recovery}$ are the uptake and recovery intervals, as defined previously. t_{uptake}

ACCEPTED MANUSCRIPT

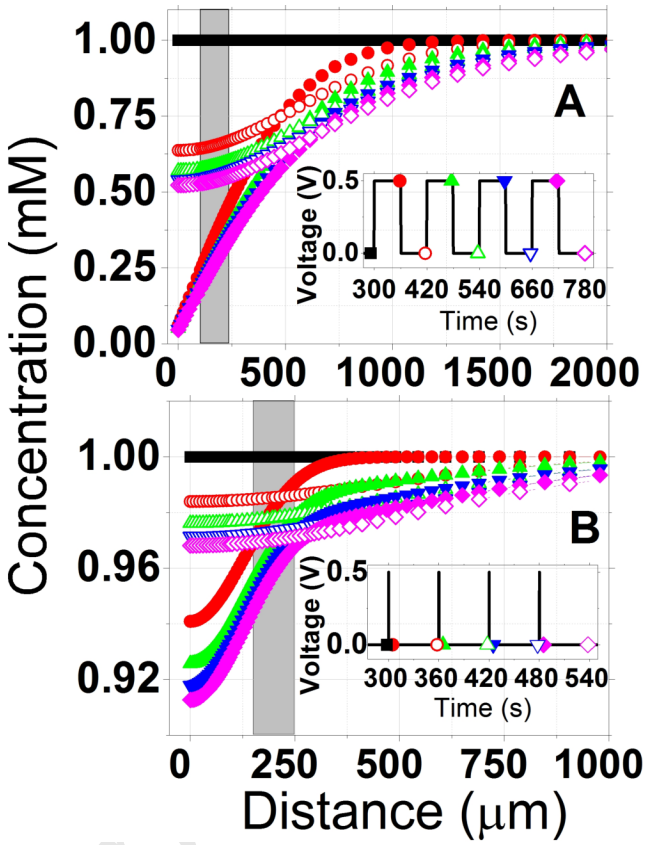


Figure 5: **Simulated concentration profiles were obtained for various time points during the potential pulse waves applied to the LSE. Each pulse wave comprises four pulses. Despite being identical, the pulses yield concentration profiles that differ quantitatively from one pulse to another, due to partial recovery of the concentration profile before starting a new pulse.** Plotted curves indicate simulated concentration profiles as functions of distance along the z-axis (LSE is at z = 0) and for various time points indicated by symbols in the insets. Curves in the insets indicate potential pulse waves ($t_{pulse} = t_{uptake} + t_{recovery}$) applied to the LSE with (A) t_{uptake} = 60 s and (B) t_{uptake} = 0.15 s. In both cases $t_{recovery}$ = 60 s. Shaded bands (150 μm < z < 250 μm) indicate the regions occupied by the electrodes during the experiments. Since $t_{recovery}$ is the same for all pulse waves, the numerical results indicate that t_{uptake} is responsible for the magnitude of concentration change at the electrode positions during each uptake interval, and is also responsible for the transient spatial scale of the corresponding concentration fields.

ACCEPTED MANUSCRIPT

and $t_{recovery}$ are controllable parameters for excitation of the active surface. Fickian diffusion is such that, for an infinitely long uptake interval (i.e., $t_{uptake} \rightarrow \infty$, $t_{recovery} \rightarrow 0$), the general functional form boils down to $C/C_0 = f(D, z, t)$. This expression can be written in terms of the delay time t_0 as $C/C_0 = f(t/t_0)$ because D, z and t are interrelated when the mass transport is due to Fickian diffusion. Therefore, for a given D, t_0 is the time required for the ratio C/C_0 at position z to reach a given value. For instance, in the present analysis t_0 is the time at which $C/C_0 = 0.7$ at the sensor positions, where the value of 0.7 corresponds approximately to the condition at which $t_0 = {z_i}^2/2D$, with z_i being the position of electrode i. Details on this derivation are provided in the Supplementary Material (Fig. S-9).

The delay time t_0 allows to write the general abovementioned expression for the measured transient concentrations in terms of normalized times, i.e., $C/C_0 = f(t_{uptake}/t_0, t_{recovery}/t_0, t/t_0)$. This normalization allows for direct comparison between concentrations measured experimentally and concentrations obtained from simulations, without requiring experimental determination of the exact values for sensor positions and diffusion coefficient. To perform the reliability assessment, both experimental and simulated data must be normalized to the corresponding values of t_0. Experimental data for t_{uptake} of 60 s provided t_0 values of 12, 18 and 25 s for E1, E2 and E3, respectively. Similarly, t_0 values from simulated data were obtained by simulating the transient concentrations measured by electrodes at positions 165, 200, and 235 μm with respect to the LSE, in response to a pulse with t_{uptake} of 100 s, and then extracting the time at which $C/C_0 = 0.7$. Experimental data in Fig. S-9 shows that electrode positioned closer to the LSE (40, 65 and 90 μm) result in smaller values of t_0 (0.5, 1.5, and 2.5 s).

Fig. 6 shows the concentration minima $C_{min,i}$ (normalized to initial background concentration C_0) as a function of t_{uptake}/t_0, for the four studied pulse waves, and from both experimental and simulated data. $C_{min,i}$ indicates the concentration minimum associated to the i-th pulse in a pulse wave (see naming conventions in Fig. S-10 in Supplementary Material). A maximum difference of 7% relative to full concentration scale (i.e., relative to C_0) is observed between experimental and simulated results, thus quantifying the ability of the MEA to resolve the signal minima for successive pulses. It is important to note, first, that this result was obtained despite the electrode variability (21.8%) and response variability (2.5%) observed in our experiments, and second, that other works in the literature have reported similar variabilities for MEAs [41, 35, 43, 36, 42, 37, 38]. These observations indi-

ACCEPTED MANUSCRIPT

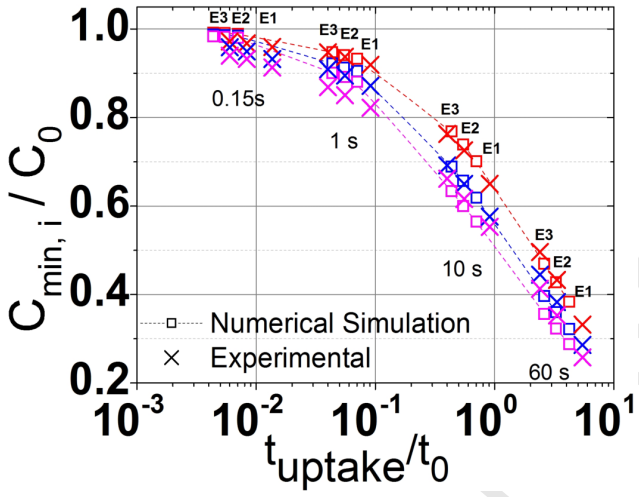


Figure 6: **Concentration minima (normalized to C_0) associated to the i-th pulse in a pulse wave are plotted as a function of t_{uptake}/t_0, for the four studied pulse waves, and from both experimental and simulated data. Normalization of the uptake interval t_{uptake} by the characteristic delay time t_0 associated to each electrode position allows for direct comparison between experimental and simulated data independently of diffusion coefficient and electrode positions. Experimental and simulated data agree quantitatively within a maximum difference of 7% relative to full concentration scale.** Red: pulse i = 1, blue: pulse i = 2, pink: pulse i = 4. C_0 is the initial background concentration, and pulse i = 3 has been omitted for clarity. Each group of points corresponds to data for the three electrodes (E1, E2, and E3) and for the indicated t_{uptake} values (0.15, 1, 10 and 60 s). Normalization of t_{uptake} by t_0 spreads and arrange the data points in the order E3, E2 and E1 from left to right in each group, consistent with t_{uptake}/t_0 being smaller for electrodes located farther from the LSE. Line connecting numerical simulation points is a guide to the eye.

cate that the in situ transient calibration is crucial to minimize the effects of sensitivity variability.

Fig. 7 shows the concentrations (normalized to C_0) at various stages of recovery (after the fourth pulse in a pulse wave) as a function of t_{uptake}/t_0, for the four studied pulse waves, and from both experimental and simulated data. The various stages of recovery are denoted by C_{R1}, C_{R2} and C_{Rf} (see Fig. S-10 in Supplementary Material), where C_{R1} is the concentration at the end of the fourth pulse, C_{R2} is the concentration after 60 s from C_{R1}, and C_{Rf} is the concentration after 200 s from C_{R1}. In this case, the difference between the experimental and simulated results is larger, particularly for later stages of the recovery, but without exceeding 15% relative to full

ACCEPTED MANUSCRIPT

concentration scale. For instance, in the case of t_{uptake} = 60 s the simulation predicts 90% of recovery, whereas the experiment exhibited 80%. In the initial stages of recovery (C_{R1} and C_{R2}), there is reasonable agreement between the experimental and simulation results. In general, the electrode response becomes saturated as it evolves from C_{R1} to C_{R2}, and finally to C_{Rf}. This effect is attributed to the signal drift in a uniform constant concentration, which is a phenomenon inherent to amperometric sensing, as observed in other reports [42, 44, 47, 48, 49]. It is important to note that this drift dominates only in conditions where the gradient of interest is either absent (i.e., in uniform constant concentration) or sluggish with respect to the signal drift rate (e.g., at later recovery stages). This observation indicates that quantitative measurements can be made with minimal errors in presence of a transient gradient that changes faster than the sensitivity drift rate.

3.7. Quantification of physiological gradient in 2D cell culture of human astrocytes

In-vitro demonstration of a physiological gradient takes advantage of the fact that 2D monolayers of astrocytes uptake H_2O_2 from the extracellular space [11, 13], thus setting up a concentration profile with associated gradients. Fig. 8 demonstrates the ability of the MEA to be positioned near the 2D cell culture and extract concentration transients at each electrode position when the cells are exposed to 20 μM H_2O_2. Due to the non-availability of a stimulus to start the uptake, a modified in situ transient calibration is employed, consisting in locating the MEA at 5 mm from the cell surface (prior to t = 330 s) to extract the calibration factors of the electrodes, and then positioning the MEA near the cells (at t = 330 s) such that the electrodes end up located at 60, 200, 340, 480 and 620 μm from the cell surface (see Fig. 8A). Fig. 8C shows the transients extracted beyond 334 s (the motion of the MEA chip takes 4 s) and indicates the presence of a gradient of H_2O_2 set up by cellular uptake, such that the order in the concentration amplitudes is E1 < E2 < E3 < E4 < E5 at any time. Fig. 8D shows the gradients and fluxes calculated from the measured transient concentrations. The concentration transients in this figure, and the corresponding gradients, were determined from single measurement runs, without averaging or smoothing.

ACCEPTED MANUSCRIPT

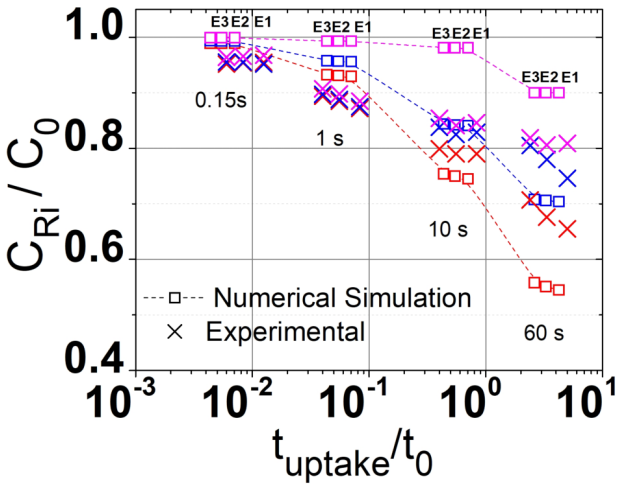


Figure 7: **Concentrations (normalized to C_0) at three time points after the fourth pulse in a pulse wave are plotted as a function of t_{uptake}/t_0, for the four studied pulse waves, and from both experimental and simulated data. Experimental and simulated data agree quantitatively within a maximum difference of 15% (relative to full concentration scale) during the illustrated stages of recovery. This increase in the difference between data sets is explained in the main text in terms of sensitivity drift.** The illustrated stages of recovery are denoted by C_{Ri} (i = 1, 2, f), where C_{R1} (red) is the concentration at the end of the fourth pulse, C_{R2} (blue) is the concentration after 60 s from C_{R1}, and C_{Rf} (pink) is the concentration after 200 s from C_{R1}. These stages quantify the final recovery when the concentrations change from $C_{R1} \rightarrow C_{R2} \rightarrow C_{Rf}$ at the electrode positions. Each group of points corresponds to data for the three electrodes (E1, E2, and E3) and for the indicated t_{uptake} values (0.15, 1, 10 and 60 s). Normalization of t_{uptake} by t_0 spreads and arrange the data points in the order E3, E2 and E1 from left to right in each group, consistent with t_{uptake}/t_0 being smaller for electrodes located farther from the LSE. Line connecting numerical simulation points is a guide to the eye.

ACCEPTED MANUSCRIPT

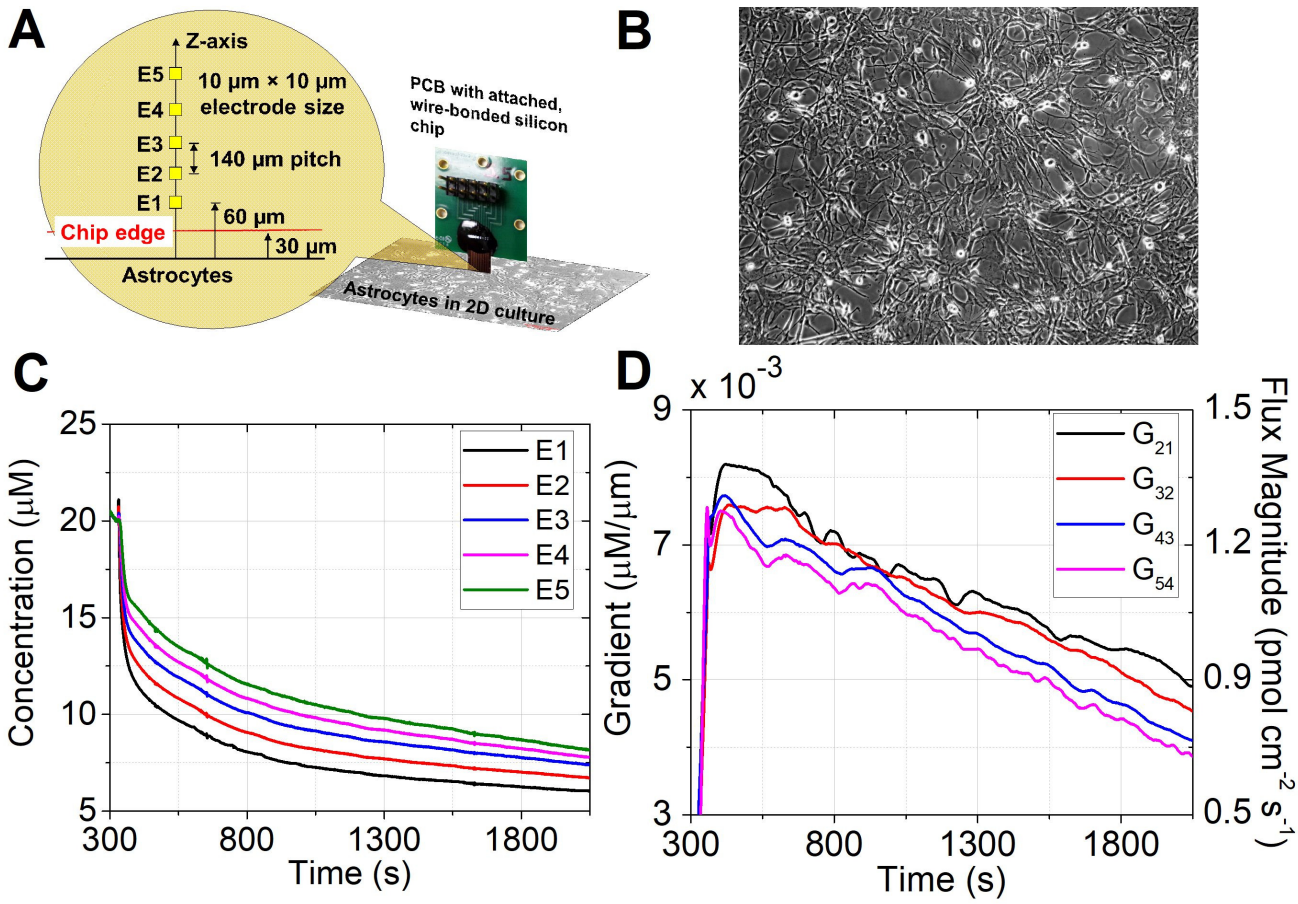


Figure 8: **On exposure to 20 μM hydrogen peroxide (H_2O_2), adherent 2D cell culture of human astrocytes continuously consumes H_2O_2, setting up an extracellular concentration gradient which is quantified using on-chip MEA and in situ transient calibration.** (A) Setup for the experiment. MEA comprises five platinum electrodes labeled E1 through E5, which are positioned at 60, 200, 340, 480 and 620 μm from the cell surface, respectively, during the transient measurements (t > 330s). As described in the text, a modified in-situ transient calibration approach involved positioning the MEA at 5 mm from the cell surface during the time interval 0<t<330 s and using the current at each electrode at t = 330 s in order to obtain a calibration factor in the presence of a uniform background concentration. (B) Photograph of the 2D culture of astrocytes seeded in a chambered cover glass well prior to H_2O_2 exposure. (C) Concentration transients measured with the five electrodes in the MEA, at the positions illustrated in (A), corresponding to H_2O_2 exposure started at t = 0. The concentration amplitudes follow the order E1 < E2 < E3 < E4 < E5, clearly indicating the presence of a dynamic gradient. (D) Gradients calculated from measured concentrations at adjacent electrodes and corresponding diffusive fluxes, which are in the range of 0.7-1.4 pmol cm^{-2} s^{-1} and decrease with time due to depletion of the local concentration.

ACCEPTED MANUSCRIPT

4. Conclusions

Sensitivity variability in amperometric sensing, and particularly in MEAs, has hindered the determination of local absolute concentrations with enough accuracy as to determine gradients based on concentration differences between closely spaced electrodes. This issue becomes worse at the smaller concentration scales found in physiological studies. In this work, we demonstrated quantitatively the measurement of transient gradients of H_2O_2 using MEAs and an active surface that controllably induces transient gradients upon excitation, and we evaluated the reliability of the measurements by comparing experimental and simulated data via normalized time analysis. The results of this analysis indicate that the in situ transient calibration, developed here, minimizes the effects of sensitivity variability to such an extent that accurate determination of local absolute concentrations is possible. Measurements demonstrated here include transient gradients caused by sub-second uptake events (using sampling time and measurement time of 10 ms, spatial range of 70 μm, and spatial resolution of 35 μm), and in vitro gradients caused by continuous H_2O_2 uptake by a 2D cell culture of human astrocytes (using spatial range of 560 μm). The diffusive fluxes associated to the measured gradients exhibited values in the range of 0.7-625 pmol cm^{-2} s^{-1}, being this a range that holds physiological relevance. Taken together, these results demonstrate the design, fabrication and application of amperometric MEAs and in situ transient calibration for the measurement of physiological gradients and fluxes in real time.

5. Acknowledgements

The authors thank The National Science Foundation (NSF Nano-biosensing Program Grant #1403582) and the Colombia-Purdue Institute for Advanced Scientific Research for supporting this work.

6. References

[1] L. F. Jaffe, R. Nuccitelli, An Ultrasensitive Vibrating Probe for Measuring Steady Extracellular Currents, J Cell Biol 63 (2) (1974) 614–628. doi:10.1083/jcb.63.2.614.
URL http://jcb.rupress.org/content/63/2/614

ACCEPTED MANUSCRIPT

[2] E. S. McLamore, S. Mohanty, J. Shi, J. Claussen, S. S. Jedlicka, J. L. Rickus, D. M. Porterfield, A self-referencing glutamate biosensor for measuring real time neuronal glutamate flux, Journal of Neuroscience Methods 189 (1) (2010) 14–22. doi:10.1016/j.jneumeth.2010.03.001.
URL http://www.sciencedirect.com/science/article/pii/S0165027010001196

[3] J. Galceran, J. Monné, J. Puy, H. P. van Leeuwen, The impact of the transient uptake flux on bioaccumulation: Linear adsorption and first-order internalisation coupled with spherical semi-infinite mass transport, Marine chemistry 85 (1) (2004) 89–102.

[4] D. Ellison, A. Mugler, M. D. Brennan, S. H. Lee, R. J. Huebner, E. R. Shamir, L. A. Woo, J. Kim, P. Amar, I. Nemenman, A. J. Ewald, A. Levchenko, Cell-cell communication enhances the capacity of cell ensembles to sense shallow gradients during morphogenesis, Proc Natl Acad Sci U S A 113 (6) (2016) E679–E688. doi:10.1073/pnas.1516503113.
URL http://www.ncbi.nlm.nih.gov/pmc/articles/PMC4760786/

[5] S. Alberghini, E. Polone, V. Corich, M. Carlot, F. Seno, A. Trovato, A. Squartini, Consequences of relative cellular positioning on quorum sensing and bacterial cell-to-cell communication, FEMS Microbiology Letters 292 (2) (2009) 149–161. doi:10.1111/j.1574-6968.2008.01478.x.
URL http://dx.doi.org/10.1111/j.1574-6968.2008.01478.x

[6] B. J. Kim, M. Wu, Microfluidics for mammalian cell chemotaxis, Annals of Biomedical Engineering 40 (6) (2012) 1316–1327. arXiv:NIHMS150003, doi:10.1007/s10439-011-0489-9.

[7] T. M. Keenan, A. Folch, Biomolecular gradients in cell culture systems, Lab Chip 8 (1) (2007) 34–57. doi:10.1039/B711887B.
URL http://pubs.rsc.org/en/content/articlelanding/2008/lc/b711887b

[8] A. G. G. Toh, Z. P. Wang, C. Yang, N.-T. Nguyen, Engineering microfluidic concentration gradient generators for biological applications, Microfluidics and Nanofluidics 16 (1) (2014) 1–18. doi:10.1007/

ACCEPTED MANUSCRIPT

s10404-013-1236-3.
URL https://doi.org/10.1007/s10404-013-1236-3

[9] S. Kim, H. J. Kim, N. L. Jeon, Biological applications of microfluidic gradient devices, Integrative Biology 2 (11-12) (2010) 584–603.

[10] E. R. Travis, Wightman, R. Mark, Spatio-Temporal Resolution of Exocytosis from Individual Cells, Annual Review of Biophysics and Biomolecular Structure 27 (1) (1998) 77–103. doi:10.1146/annurev.biophys.27.1.77.
URL http://dx.doi.org/10.1146/annurev.biophys.27.1.77

[11] S. Desagher, J. Glowinski, J. Premont, Astrocytes protect neurons from hydrogen peroxide toxicity, Journal of Neuroscience 16 (8) (1996) 2553–2562.

[12] X. Liu, M. M. Ramsey, X. Chen, D. Koley, M. Whiteley, A. J. Bard, Real-time mapping of a hydrogen peroxide concentration profile across a polymicrobial bacterial biofilm using scanning electrochemical microscopy, PNAS 108 (7) (2011) 2668–2673. doi:10.1073/pnas.1018391108.
URL http://www.pnas.org/content/108/7/2668

[13] B. A. Wagner, J. R. Witmer, T. J. van't Erve, G. R. Buettner, An assay for the rate of removal of extracellular hydrogen peroxide by cells, Redox Biology 1 (1) (2013) 210–217. doi:10.1016/j.redox.2013.01.011.
URL http://www.sciencedirect.com/science/article/pii/S2213231713000323

[14] A. Bagulho, F. Vilas-Boas, A. Pena, C. Peneda, F. C. Santos, A. Jerónimo, R. F. M. de Almeida, C. Real, The extracellular matrix modulates H_2O_2 degradation and redox signaling in endothelial cells, Redox Biology 6 (2015) 454–460. doi:10.1016/j.redox.2015.09.006.
URL http://www.sciencedirect.com/science/article/pii/S2213231715001172

[15] H. S. Marinho, L. Cyrne, E. Cadenas, F. Antunes, H_2O_2 Delivery to Cells, Methods in Enzymology 526 (2013) 159 – 173, hydrogen Peroxide and Cell Signaling, Part A. doi:http://dx.doi.org/10.1016/B978-0-12-405883-5.00010-7.

Accepted Manuscript

ACCEPTED MANUSCRIPT

URL http://www.sciencedirect.com/science/article/pii/B9780124058835000107

[16] L. M. Kauri, S.-K. Jung, R. T. Kennedy, Direct measurement of glucose gradients and mass transport within islets of langerhans, Biochemical and biophysical research communications 304 (2) (2003) 371–377.

[17] D. M. Porterfield, Measuring metabolism and biophysical flux in the tissue, cellular and sub-cellular domains: Recent developments in self-referencing amperometry for physiological sensing, Biosensors and Bioelectronics 22 (7) (2007) 1186–1196. doi:10.1016/j.bios.2006.06.006.
URL http://www.sciencedirect.com/science/article/pii/S0956566306002740

[18] Q. Wu, M. E. Reith, R. M. Wightman, K. T. Kawagoe, P. A. Garris, Determination of release and uptake parameters from electrically evoked dopamine dynamics measured by real-time voltammetry, Journal of neuroscience methods 112 (2) (2001) 119–133.

[19] C. F. Ng, F. Q. Schafer, G. R. Buettner, V. Rodgers, The rate of cellular hydrogen peroxide removal shows dependency on gsh: mathematical insight into in vivo H_2O_2 and gpx concentrations, Free radical research 41 (11) (2007) 1201–1211.

[20] S. H. Walters, I. M. Taylor, Z. Shu, A. C. Michael, A novel restricted diffusion model of evoked dopamine, ACS chemical neuroscience 5 (9) (2014) 776–783.

[21] A. I. Oleinick, C. Amatore, M. Guille, S. Arbault, O. V. Klymenko, I. Svir, Modelling release of nitric oxide in a slice of rat's brain: describing stimulated functional hyperemia with diffusion-reaction equations, Mathematical Medicine and Biology 23 (1) (2006) 27–44.

[22] W. M. Kühtreiber, L. F. Jaffe, Detection of extracellular calcium gradients with a calcium-specific vibrating electrode., The Journal of cell biology 110 (5) (1990) 1565–1573.

[23] S.-K. Jung, J. R. Trimarchi, R. H. Sanger, P. J. Smith, Development and application of a self-referencing glucose microsensor for the measure-

ACCEPTED MANUSCRIPT

ment of glucose consumption by pancreatic β-cells, Analytical chemistry 73 (15) (2001) 3759–3767.

[24] J. Shi, E. S. McLamore, D. Jaroch, J. C. Claussen, R. G. Mirmira, J. L. Rickus, D. M. Porterfield, Oscillatory glucose flux in ins 1 pancreatic β cells: A self-referencing microbiosensor study, Analytical biochemistry 411 (2) (2011) 185–193.

[25] E. McLamore, J. Shi, D. Jaroch, J. Claussen, A. Uchida, Y. Jiang, W. Zhang, S. Donkin, M. Banks, K. Buhman, D. Teegarden, J. Rickus, D. Porterfield, A self referencing platinum nanoparticle decorated enzyme-based microbiosensor for real time measurement of physiological glucose transport, Biosensors and Bioelectronics 26 (5) (2011) 2237 – 2245. doi:http://dx.doi.org/10.1016/j.bios.2010.09.041.
URL http://www.sciencedirect.com/science/article/pii/S095656631000655X

[26] N. Baltes, L. Thouin, C. Amatore, J. Heinze, Imaging Concentration Profiles of Redox Active Species with Nanometric Amperometric Probes: Effect of Natural Convection on Transport at Microdisk Electrodes, url = http://onlinelibrary.wiley.com/doi/10.1002/anie.200352662/abstract, volume = 43, year = 2004, Angewandte Chemie International Edition (11) 1431–1435. doi:10.1002/anie.200352662.

[27] R. Chen, K. Hu, Y. Yu, M. V. Mirkin, S. Amemiya, Focused-ion-beam-milled carbon nanoelectrodes for scanning electrochemical microscopy, Journal of The Electrochemical Society 163 (4) (2016) H3032–H3037.

[28] T. Sun, Y. Yu, B. J. Zacher, M. V. Mirkin, Scanning electrochemical microscopy of individual catalytic nanoparticles, Angewandte Chemie International Edition 53 (51) (2014) 14120–14123.

[29] S. Amemiya, A. J. Bard, F.-R. F. Fan, M. V. Mirkin, P. R. Unwin, Scanning electrochemical microscopy, Annu. Rev. Anal. Chem. 1 (2008) 95–131.

[30] P. Sun, F. O. Laforge, M. V. Mirkin, Scanning electrochemical microscopy in the 21st century, Physical Chemistry Chemical Physics 9 (7) (2007) 802–823.

ACCEPTED MANUSCRIPT

[31] S. M. Oja, Y. Fan, C. M. Armstrong, P. Defnet, B. Zhang, Nanoscale electrochemistry revisited, Analytical Chemistry 88 (1) (2016) 414–430, pMID: 26630546. arXiv:http://dx.doi.org/10.1021/acs.analchem.5b04542, doi:10.1021/acs.analchem.5b04542.
URL http://dx.doi.org/10.1021/acs.analchem.5b04542

[32] C. Amatore, A. Chovin, P. Garrigue, L. Servant, N. Sojic, S. Szunerits, L. Thouin, Remote fluorescence imaging of dynamic concentration profiles with micrometer resolution using a coherent optical fiber bundle, Analytical Chemistry 76 (24) (2004) 7202–7210, pMID: 15595861. arXiv:http://dx.doi.org/10.1021/ac049017g, doi:10.1021/ac049017g.
URL http://dx.doi.org/10.1021/ac049017g

[33] S. G. Rhee, T.-S. Chang, W. Jeong, D. Kang, Methods for detection and measurement of hydrogen peroxide inside and outside of cells, Molecules and cells 29 (6) (2010) 539–549.

[34] K. Y. Inoue, M. Matsudaira, R. Kubo, M. Nakano, S. Yoshida, S. Matsuzaki, A. Suda, R. Kunikata, T. Kimura, R. Tsurumi, et al., Lsi-based amperometric sensor for bio-imaging and multi-point biosensing, Lab on a Chip 12 (18) (2012) 3481–3490.

[35] J. B. Wydallis, R. M. Feeny, W. Wilson, T. Kern, T. Chen, S. Tobet, M. M. Reynolds, C. S. Henry, Spatiotemporal norepinephrine mapping using a high-density CMOS microelectrode array, Lab Chip 15 (20) (2015) 4075–4082. doi:10.1039/C5LC00778J.
URL http://pubs.rsc.org/en/content/articlelanding/2015/lc/c5lc00778j

[36] B. N. Kim, A. D. Herbst, S. J. Kim, B. A. Minch, M. Lindau, Parallel recording of neurotransmitters release from chromaffin cells using a 10×10 CMOS IC potentiostat array with on-chip working electrodes, Biosensors and Bioelectronics 41 (2013) 736–744. doi:10.1016/j.bios.2012.09.058.
URL http://www.sciencedirect.com/science/article/pii/S0956566312006641

[37] J. Rothe, O. Frey, A. Stettler, Y. Chen, A. Hierlemann, Fully integrated cmos microsystem for electrochemical measurements on 32× 32 working

ACCEPTED MANUSCRIPT

electrodes at 90 frames per second, Analytical chemistry 86 (13) (2014) 6425–6432.

[38] H. Meyer, H. Drewer, B. Gruendig, K. Cammann, R. Kakerow, Y. Manoli, W. Mokwa, M. Rospert, Two-dimensional imaging of o2, h2o2, and glucose distributions by an array of 400 individually addressable microelectrodes, Analytical Chemistry 67 (7) (1995) 1164–1170.

[39] J. Wang, R. Trouillon, J. Dunevall, A. G. Ewing, Spatial resolution of single-cell exocytosis by microwell-based individually addressable thin film ultramicroelectrode arrays, Analytical chemistry 86 (9) (2014) 4515–4520.

[40] J. Wigström, J. Dunevall, N. Najafinobar, J. Lovrić, J. Wang, A. G. Ewing, A.-S. Cans, Lithographic microfabrication of a 16-electrode array on a probe tip for high spatial resolution electrochemical localization of exocytosis, Analytical chemistry 88 (4) (2016) 2080–2087.

[41] J. Yan, V. A. Pedrosa, J. Enomoto, A. L. Simonian, A. Revzin, Electrochemical biosensors for on-chip detection of oxidative stress from immune cells, Biomicrofluidics 5 (3) (2011) 032008.

[42] M. Şen, K. Ino, K. Y. Inoue, T. Arai, T. Nishijo, A. Suda, R. Kunikata, H. Shiku, T. Matsue, Lsi-based amperometric sensor for real-time monitoring of embryoid bodies, Biosensors and Bioelectronics 48 (2013) 12–18.

[43] J. Wang, R. Trouillon, Y. Lin, M. I. Svensson, A. G. Ewing, Individually addressable thin-film ultramicroelectrode array for spatial measurements of single vesicle release, Analytical chemistry 85 (11) (2013) 5600–5608.

[44] H. Abe, K. Ino, C.-Z. Li, Y. Kanno, K. Y. Inoue, A. Suda, R. Kunikata, M. Matsudaira, Y. Takahashi, H. Shiku, et al., Electrochemical imaging of dopamine release from three-dimensional-cultured pc12 cells using large-scale integration-based amperometric sensors, Analytical chemistry 87 (12) (2015) 6364–6370.

[45] C. Amatore, J. Delacotte, M. Guille-Collignon, F. Lemaître, Vesicular exocytosis and microdevices–microelectrode arrays, Analyst 140 (11) (2015) 3687–3695.

ACCEPTED MANUSCRIPT

[46] F. Picollo, A. Battiato, E. Bernardi, A. Marcantoni, A. Pasquarelli, E. Carbone, P. Olivero, V. Carabelli, Microelectrode arrays of diamond-insulated graphitic channels for real-time detection of exocytotic events from cultured chromaffin cells and slices of adrenal glands, Analytical chemistry 88 (15) (2016) 7493–7499.

[47] Y. Zhang, G. S. Wilson, Electrochemical oxidation of h2o2 on pt and pt+ ir electrodes in physiological buffer and its applicability to h2o2-based biosensors, Journal of Electroanalytical Chemistry 345 (1-2) (1993) 253–271.

[48] S. A. Evans, J. M. Elliott, L. M. Andrews, P. N. Bartlett, P. J. Doyle, G. Denuault, Detection of hydrogen peroxide at mesoporous platinum microelectrodes, Analytical Chemistry 74 (6) (2002) 1322–1326.

[49] S. R. Belding, E. I. Rogers, R. G. Compton, Potential step chronoamperometry at microdisc electrodes: effect of finite electrode kinetics, The Journal of Physical Chemistry C 113 (10) (2009) 4202–4207.

[50] N. G. Poulos, J. R. Hall, M. C. Leopold, Functional layer-by-layer design of xerogel-based first-generation amperometric glucose biosensors, Langmuir 31 (4) (2015) 1547–1555.

[51] J. Rothe, M. Lewandowska, F. Heer, O. Frey, A. Hierlemann, Multi-target electrochemical biosensing enabled by integrated cmos electronics, Journal of Micromechanics and Microengineering 21 (5) (2011) 054010.

[52] C. F. Lourenço, A. Ledo, J. Laranjinha, G. A. Gerhardt, R. M. Barbosa, Microelectrode array biosensor for high-resolution measurements of extracellular glucose in the brain, Sensors and Actuators B: Chemical 237 (2016) 298–307.

[53] D. M. H. Kern, The Polarography and Standard Potential of the Oxygen-Hydrogen Peroxide Couple, J. Am. Chem. Soc. 76 (16) (1954) 4208–4214. doi:10.1021/ja01645a059.
URL http://dx.doi.org/10.1021/ja01645a059

[54] C. Amatore, S. Arbault, D. Bruce, P. de Oliveira, M. Erard, M. Vuillaume, Analysis of individual biochemical events based on artificial synapses using ultramicroelectrodes: cellular oxidative burst, Faraday

Accepted Manuscript

ACCEPTED MANUSCRIPT

Discuss. 116 (0) (2000) 319–333. doi:10.1039/B001448F.
URL http://pubs.rsc.org/en/content/articlelanding/2000/fd/b001448f

[55] C. Amatore, S. Arbault, D. Bruce, P. De Oliveira, M. Erard, N. Sojic, M. Vuillaume, Nitrogen monoxide and oxidative stress: composition and intensity of cellular oxidative bursts cocktail. a study through artificial electrochemical synapses on single human fibroblasts, Analusis 28 (6) (2000) 506–517.

[56] C. Amatore, S. Arbault, C. Bouton, K. Coffi, J.-C. Drapier, H. Ghandour, Y. Tong, Monitoring in real time with a microelectrode the release of reactive oxygen and nitrogen species by a single macrophage stimulated by its membrane mechanical depolarization, ChemBioChem 7 (4) (2006) 653–661.

[57] V. Folmer, N. Pedroso, A. C. Matias, S. C. Lopes, F. Antunes, L. Cyrne, H. S. Marinho, H 2 o 2 induces rapid biophysical and permeability changes in the plasma membrane of saccharomyces cerevisiae, Biochimica et Biophysica Acta (BBA)-Biomembranes 1778 (4) (2008) 1141–1147.

[58] D. Erudaitius, A. Huang, S. Kazmi, G. R. Buettner, V. G. Rodgers, Peroxiporin expression is an important factor for cancer cell susceptibility to therapeutic h2o2: Implications for pharmacological ascorbate therapy, PloS one 12 (1) (2017) e0170442.

[59] D. Suazo-Dávila, J. Rivera-Meléndez, J. Koehne, M. Meyyappan, C. R. Cabrera, Surface analysis and electrochemistry of a robust carbon-nanofiber-based electrode platform h2o2 sensor, Applied Surface Science 384 (Supplement C) (2016) 251 – 257. doi:https://doi.org/10.1016/j.apsusc.2016.05.027.
URL http://www.sciencedirect.com/science/article/pii/S0169433216310339

[60] B. I. Rosario-Castro, E. J. Contés-de Jesús, M. Lebrón-Colón, M. A. Meador, M. A. Scibioh, C. R. Cabrera, Single-wall carbon nanotube chemical attachment at platinum electrodes, Applied Surface Science 257 (2) (2010) 340–353.

ACCEPTED MANUSCRIPT

[61] B. Day, F. Pomerleau, J. Burmeister, P. Huettl, G. Gerhardt, Microelectrode array studies of basal and potassium-evoked release of l-glutamate in the anesthetized rat brain, Journal of neurochemistry 96 (6) (2006) 1626–1635.

[62] R. Madangopal, M. Stensberg, M. Porterfield, J. Rickus, N. Pulliam, Directed enzyme deposition via electroactive polymer-based nanomaterials for multi-analyte amperometric biosensors, in: 2012 IEEE Sensors, 2012, pp. 1–4. doi:10.1109/ICSENS.2012.6411166.

[63] H. Sies, Hydrogen peroxide as a central redox signaling molecule in physiological oxidative stress: oxidative eustress, Redox biology.

[64] S. S. Jedlicka, M. Dadarlat, T. Hassell, Y. Lin, A. Young, M. Zhang, P. Irazoqui, J. L. Rickus, Calibration of neurotransmitter release from neural cells for therapeutic implants, International journal of neural systems 19 (03) (2009) 197–212.

[65] P. Nair, M. Alam, Performance limits of nanobiosensors, Applied physics letters 88 (23) (2006) 233120.

[66] A. J. Bard, L. R. Faulkner, et al., Electrochemical Methods: Fundamentals and applications, Vol. 2, Wiley New York, 2001.

[67] L. Rajendran, Modelling of reaction–diffusion processes: the theory of catalytic electrode processes at hemispheroidal ultramicroelectrodes, Electrochemistry communications 2 (10) (2000) 679–684.

[68] S. Loghambal, L. Rajendran, Mathematical modeling of diffusion and kinetics in amperometric immobilized enzyme electrodes, Electrochimica Acta 55 (18) (2010) 5230–5238.

[69] P. R. Nair, M. A. Alam, A compact analytical formalism for current transients in electrochemical systems, Analyst 138 (2) (2013) 525–538.

[70] R. C. Engstrom, M. Weber, D. J. Wunder, R. Burgess, S. Winquist, Measurements within the diffusion layer using a microelectrode probe, Anal. Chem. 58 (4) (1986) 844–848. doi:10.1021/ac00295a044.
URL http://pubs.acs.org/doi/abs/10.1021/ac00295a044

ACCEPTED MANUSCRIPT

Research Highlights

- Developed on-chip MEA to address gradient measurements in 2D cell culture setups.
- Developed in-situ transient calibration for minimizing sensitivity variability in MEAs
- Assessed reliability of dynamic gradient measurements using large sink electrode that mimics cellular uptake.
- Measured gradients from uptake intervals as short as 150 ms, and up to 2000 s.
- Measured physiological dynamic gradient due to H_2O_2 uptake by human astrocytes.

Accepted Manuscript

ACCEPTED MANUSCRIPT

Include in the manuscript a short (maximum 100 words) biography of each author.

Siddarth V. Sridharan. Mr. Sridharan received his B.Tech. degree in Electrical and Communication Engineering from SRM University, Chennai, India. He is currently a Ph.D candidate in School of Electrical and Computer Engineering, Purdue University, West Lafayette, IN, USA. His current research interests include fabrication and development of multi analyte bio-sensor arrays for measurement of analyte flux and mapping concentration profiles from 2D/3D cell cultures. His work also focuses on numerical simulations of reaction-diffusion models involving UMEs in order to improve the design and performance of sensor arrays.

Jose Ferney Rivera. Mr. Rivera received B.Sc. and M.Sc. degrees both in Electronics Engineering from Universidad del Valle, Cali, Colombia. He is currently a Ph.D. candidate in School of Electrical and Computer Engineering, Purdue University, West Lafayette, IN, USA. His research focuses on design, modeling, fabrication, and characterization of nano- and micro-systems for detection of gases and measurement of biophysical fluxes.

James Nolan. Mr. Nolan received his B.S. in Biological Engineering from Purdue University, West Lafayette, IN, USA, in 2015. He is currently a M.S. candidate in the Department of Agricultural and Biological Engineering, Purdue University. His research is on physiological sensing and miniaturization of biofuel cells.

Muhammad Ashraful Alam. Professor Alam holds the Jai N. Gupta endowed chair professorship at Purdue University, where his research focuses on the physics and technology of semiconductor devices. From 1995 to 2003, he was with Bell Laboratories, Murray Hill, NJ working on optoelectronic integrated circuits. Since joining Purdue in 2004, Dr. Alam has published over 300 papers on biosensors, transistors, solar cells, and flexible electronics. He is a fellow of IEEE, APS, and AAAS. His awards include the 2006 IEEE Kiyo Tomiyasu Medal for contributions to device technology and 2015 SRC Technical Excellence Award for fundamental contributions to reliability physics.

Jenna L. Rickus. Professor Rickus received the Ph.D. degree at University of California, Los Angeles, CA, USA, in 2003. She is a Professor in the Department of Agricultural and Biological Engineering and the Weldon School of Engineering and the Associate Vice Provost for Teaching and Learning at Purdue University. Her research focuses on biofunctional materials for biosensors and biointerfaces with a focus on applications related to the brain and pancreas. She is currently a fellow of ELATE (Executive Leadership on Academic Technology and Engineering).

David B. Janes. Professor Janes received the B.A. degree in Physics from Augustana College in 1980 and the B.S.E.E., M.S.E.E. and Ph.D. degrees from the University of Illinois at Urbana-Champaign in 1980, 1981 and 1989, respectively. From 1981 to 1985, he worked as a research scientist at the Research Division of Raytheon Company, where he worked on microwave devices and integrated circuits. Since 1989, he has been at Purdue University, where he is a Professor of Electrical and Computer Engineering. He is engaged in experimental studies on biosensors, nanoelectronic devices and nanostructured transparent conductors.